MSNG-2025

SİVAS CUMHURİYET ÜNİVERSİTESİ 1974

12th INTERNATIONAL CONFERENCE ON MATERIALS SCIENCE AND NANOTECHNOLOGY FOR NEXT GENERATION

(MSNG2025)

10-12 September 2025

SİVAS CUMHURİYET UNIVERSITY

FULL TEXT BOOK

Editors

- Prof. Dr. Fahrettin Yakuphanoğlu
- Prof. Dr. Ebru Şenadım Tüzemen
- Prof. Dr. Ahmet Ekicibil
- Assoc. Prof. Dr. Ahmet Türker Tüzemen
- Assoc. Prof. Dr. Ayşegül Dere

SİVAS CUMHURİYET ÜNİVERSİTESİ

Full Text Book - 12th International Conference on Materials Science and Nanotechnology for Next Generation (MSNG2025)

ISBN
978-625-6497-70-2

Editörler
Prof. Dr. Fahrettin Yakuphanoğlu
Prof. Dr. Ebru Şenadım Tüzemen
Prof. Dr. Ahmet Ekicibil
Assoc. Prof. Dr. Ahmet Türker Tüzemen
Assoc. Prof. Dr. Ayşegül Dere

Kapak ve İç Düzen
Abdulkadir Kocatürk

Baskı
Sivas Cumhuriyet Üniversitesi Rektörlük Matbaa
Sertifika No: 40954

Dağıtım
Sivas Cumhuriyet Üniversitesi

Sivas / Ekim - 2025

SİVAS CUMHURİYET ÜNİVERSİTESİ YAYINLARI No: 333
16/10/2025 tarih ve 17 numaralı Sivas Cumhuriyet Üniversitesi Yayın Kurulu Kararı ile 31/10/2025 tarih ve 35 numaralı Sivas Cumhuriyet Üniversitesi Yönetim Kurulu Kararına istinaden basımı uygun görülmüştür.

CONTENTS

COMMITEES

HONORARY PRESIDENTS

Prof. Dr. Ahmet Şengönül	Rector of Sivas Cumhuriyet University / Türkiye
Prof. Dr. Fahrettin Göktaş	Rector of Fırat University / Türkiye

CONFERENCE PRESIDENTS

Prof. Dr. Fahrettin Yakuphanoğlu	Fırat University / Türkiye
Prof. Dr. Ebru Şenadım Tüzemen	Sivas Cumhuriyet University / Türkiye

ORGANIZING COMMITTEE

Ahmet Ekicibil	Çukurova University / Türkiye
Faruk Karadağ	Çukurova University / Türkiye
Serkan Akkoyun	Sivas Cumhuriyet University / Türkiye
Esin Kasapoğlu	Sivas Cumhuriyet University / Türkiye
Emine Öztürk	Sivas Cumhuriyet University / Türkiye
Rana Özbakır	Sivas Cumhuriyet University / Türkiye
Fatih Ungan	Sivas Cumhuriyet University / Türkiye
Ali Osman Ayaş	Adıyaman University / Türkiye
Ahmet Türker Tüzemen	Sivas Cumhuriyet University / Türkiye
İlkay Demir	Sivas Cumhuriyet University / Türkiye
Ayşegül Dere	Fırat University / Türkiye
Doğan Kaya	Çukurova University / Türkiye
Rachid Thaljaoui	Monastir University / Tunisia
Burhan Coşkun	Kırklareli University / Türkiye

EDITORS OF FULL TEXT BOOK

Prof. Dr. Fahrettin Yakuphanoğlu	Fırat University / Türkiye
Prof. Dr. Ebru Şenadım Tüzemen	Sivas Cumhuriyet University / Türkiye
Prof. Dr. Ahmet Ekicibil	Çukurova University / Türkiye
Assoc. Prof. Dr. Ahmet Türker Tüzemen	Sivas Cumhuriyet University / Türkiye
Assoc. Prof. Dr. Ayşegül Dere	Fırat University / Türkiye

SCIENTIFIC COMMITTEE

1.	Abdulkarim Amirov	Immanuel Kant Baltic Federal University /Russia
2.	Abdulkerim Karabulut	Erzurum Teknik University / Türkiye
3.	Adem Tataroğlu	Gazi University / Türkiye
4.	Adnan Özdemir	Kahramanmaraş İstiklal University / Türkiye
5.	Adrian M.T. Sılva	University of Porto / Portugal
6.	Ahmet Ekicibil	Çukurova University / Türkiye
7.	Ahmet Faruk Özdemir	Süleyman Demirel University / Türkiye
8.	Ahmet Oral	Middle East Technical University / Türkiye
9.	Ahmet Türker Tüzemen	Sivas Cumhuriyet University / Türkiye
10.	Ali Abdolahzadeh Ziabari	Lahijan Branch, Islamic Azad University / Iranian
11.	Ali Coşkun	University of Fribourg / Switzerland
12.	Ali Kemal Havare	Toros University / Türkiye
13.	Ali Osman Ayaş	Adıyaman University / Türkiye
14.	Ali Suat Yıldız	Sivas University of Sci. And Technology/ Türkiye
15.	Arif Kösemen	Muş Alparslan University / Türkiye
16.	Arife Gencer İmer	Van Yüzüncü Yıl University / Türkiye
17.	Atilla Coşkun	Muğla Sıtkı Koçman University / Türkiye
18.	Bekir Özçelik	Çukurova University / Türkiye
19.	Berna Bülbül	Balıkesir University / Türkiye
20.	Berrin Özdemir	Çukurova University / Türkiye
21.	Betül Kakfaslıoğlu Yıldız	Sivas University of Sci. and Technology / Türkiye
22.	Bilgehan Güzel	Çukurova University / Türkiye
23.	Buket Saatçi	Erciyes University / Türkiye
24.	Burhan Coşkun	Kırklareli University / Türkiye
25.	Bünyemin Coşut	Gebze Technical University / Türkiye
26.	Byeong-Kwon Ju	Korea University / Korea
27.	Cem Çelebi	İzmir Institute of Technology / Türkiye
28.	Ceren Orak	Sivas University of Sci. And Technology / Türkiye
29.	Cevher Ak	Toros University / Türkiye
30.	Christian Wenger	Innov. for High Performance Microelect./ Germany
31.	Christoph Stampfer	USA RWTH Aachen University / Germany
32.	Chung Gwıy-Sang	Ulsan University / Korea
33.	Cumali Sabah	Middle East Tech. University / Northern Cyprus
34.	D. D. Zaıtsev	Moscow State University / Russia
35.	D. Esra Yıldız	Hitit University / Türkiye
36.	D. S. Patıl	North Maharashtra University / India
37.	Darina Arsova	Institute of Solid State Physics / Bulgaria
38.	Denis Nika	Moldova University / Moldova
39.	Deniz Sunar Çerçi	Yıldız Technical University / Türkiye
40.	Dever Norman	Henderson State University / USA
41.	Dionysios Dionysiou	University of Cincinnati / USA
42.	Doğan Kaya	Çukurova University / Türkiye

43.	E. Hassan Aly	Ain Shams University / Egypt
44.	Ebru Şenadım Tüzemen	Sivas Cumhuriyet University / Türkiye
45.	Ebru Yabaş	Sivas Cumhuriyet University / Türkiye
46.	Elias Stathatos	Tecnological-Educational Inst. of Patras / Greece
47.	Emine Aldırmaz	Amasya University / Türkiye
48.	Emine Güneri	Erciyes University / Türkiye
49.	Emine Öztürk	Sivas Cumhuriyet University / Türkiye
50.	Emmanuel Koudoumas	Tech. Educational Institute of Crete / Greece
51.	Emmanuel Kymakis	Tech. Educational Institute of Crete / Greece
52.	Emre Bahadır Al	Sivas Cumhuriyet University / Türkiye
53.	Emre Ozan Polat	ICFO-The Institute of Photonic Sciences / Spain
54.	Esin Kasapoğlu	Sivas Cumhuriyet University / Türkiye
55.	Esra Alveroğlu	Istanbul Technical University / Türkiye
56.	Evangelos Vitoratos	University of Patras / Greece
57.	Faruk Karadağ	Çukurova University / Türkiye
58.	Fatih Ungan	Sivas Cumhuriyet University / Türkiye
59.	Fatma Göde	Mehmet Akif Ersoy University / Türkiye
60.	Feng Hua Zhang	Nanyang Technological University / Singapore
61.	Ferda Mindivan	Bilecik Şeyh Edebali University / Türkiye
62.	Fikret Işık	Trakya University / Türkiye
63.	Filiz Şenkal	Istanbul Technical University /Türkiye
64.	Fumihiko Hirose	Yamagata University / Japan
65.	Gabriel Constantinescui	University of Aveiro / Portugal
66.	Gamze Barım	Adıyaman University / Türkiye
67.	Giorgio Sberveglieri	University of Brescia / Italy
68.	Gökhan Demirel	Gazi University / Türkiye
69.	Gönül Akça	Çukurova University / Türkiye
70.	Grzegorz Karczewski	Polish Academy of Sciences / Poland
71.	H. Ghanem	Fayoum University Fayoum / Egypt
72.	Habibe Uslu Tecimer	Karabük University / Türkiye
73.	Hadi Heidari	University of Glasgow / United Kingdom
74.	Haluk Koralay	Gazi, University / Türkiye
75.	Harun Mindivan	Bilecik Şeyh Edebali University / Türkiye
76.	Hülya Doğan	Sivas Cumhuriyet University / Türkiye
77.	Hülya Metin Gübür	Mersin University / Türkiye
78.	Hüseyin Tecimer	Karabük University / Türkiye
79.	Hwan Kyu Kim	Korea University / Korea
80.	Hye-Won Seo	Jeju National University / South Korea
81.	İbrahim Erol	Afyon Kocatepe University / Türkiye
82.	İbrahim İnanç	19 Mayıs University / Türkiye
83.	İlkay Demir	Sivas Cumhuriyet University / Türkiye
84.	İlker Doğan	The Netherlands Organisation / Netherlands
85.	İmran Avcı	VU-University of Amsterdam/ Netherlands
86.	İskender Özkul	Mersin University / Türkiye

87.	İsmail Altuntaş	Sivas Cumhuriyet University / Türkiye
88.	Jingkun Xu	Technology Normal University / China
89.	Jongeun Ryu	Portugal University of California / USA
90.	José M. Kenny	University of Perugia / Italy
91.	Juan Carlos Martinez-Anton	Complutense University of Madrid / Spain
92.	Kamuran Görgün	Eskişehir Osmangzi University / Türkiye
93.	Kasım Ocakoğlu	Tarsus University / Türkiye
94.	Katerina Pomoni	University of Patras / Greece
95.	Khasan S. Karimov	GIK Institute / Pakistan
96.	Kristina Rusimova	University of Bath / United Kingdom
97.	Kübra Yakıncı	İskendurun Technical University / Türkiye
98.	Lee Xinliang	Technische Universitat Dresden / Germany
99.	Luis Banares	Universidad Complutense de Madrid / Spain
100.	Luisa Torsi	Universita Bari Aldo Moro / Italy
101.	M. Eyyüphan Yakıncı	İskenderun Technical University / Türkiye
102.	Mahmut Kuş	Konya Technical University / Türkiye
103.	Marco Antonio Schiavon	Universidade Federal de São João Del Rei / Brazil
104.	Mehmet Acet	University of Duisburg-Essen / Germany
105.	Mehmet Enver Aydın	Dicle University / Türkiye
106.	Mehmet Gürsul	Çukurova University / Türkiye
107.	Mehmet Karakılçık	Çukurova University / Türkiye
108.	Mehmet Sait Bozgeyik	Kahramanmaraş Sütçü İmam University / Türkiye
109.	Merih Palandöken	İzmir Katip Çelebi University / Türkiye
110.	Merve Özcan	Toros University / Türkiye
111.	Meryem Derya Alyörük	Aksaray University / Türkiye
112.	Metin Özdemir	Çukurova University / Türkiye
113.	Michal Babij	University of Wroclaw / Poland
114.	Mikhail I. Vasilevskiy	University of Minho / Portugal
115.	Mohamed Bououdina	Univeristy of Bahrain / Kingdom Of Bahrain
116.	Muhammad Atıf	King Saud University Riyadh / Saudi Arabia
117.	Muhammad Hassan Sayyad	Ghulam Ishaq Khan Institute / Pakistan
118.	Muharrem Karaaslan	Iskenderun Technical University / Türkiye
119.	Muhittin Doğan	Gaziantep University / Turkiye
120.	Mujdat Çağlar	Eskişehir Technical University / Türkiye
121.	Murat Köksal	Sivas Cumhuriyet University / Türkiye
122.	Murat Soylu	Bingöl University / Türkiye
123.	Mustafa Akyol	Alparslan Türkeş Sci. and Tech. University/Türkiye
124.	Mustafa Erkovan	Sakarya University / Türkiye
125.	Mustafa Kemal Bahar	Sivas Cumhuriyet University / Türkiye
126.	Mustafa Tepe	Ege University / Türkiye
127.	Nadir Dizge	Mersin University / Türkiye
128.	Nihat Tuğluoğlu	Giresun University / Türkiye
129.	Nourah Al Senany	King Abdulaziz University / Saudi Arabia
130.	Nouredine Sengouga	Université de Biskra / Algeria

131.	Oğuzhan Akgöl	İskenderun Technical University / Türkiye
132.	Osman Dayan	Çanakkale Onsekiz Mart University / Türkiye
133.	Önder Metin	Koç University / Türkiye
134.	Panagiotis Lianos	University of Patras / Greece
135.	Pedram Khalili Amiri	Northwestern University / USA
136.	Pınar Başer	Sivas Cumhuriyet University / Türkiye
137.	Polycarpos Falaras	Scientific Research Center / Greece
138.	Quanmin Guo	University of Birmingham / United Kingdom
139.	Quentin M. Ramasse	University of Liverpool / United Kingdom
140.	R. O. Ocaya	University of Free State / South Africa
141.	Rachid Thaljaoui	Monastir University / Tunisia
142.	Ram K. Gupta	Pittsburg State University / USA
143.	Ramin Yousefi	Islamic Azad University / Iranian
144.	Rana Özbakır	Sivas Cumhuriyet University / Türkiye
145.	Raşit Turan	Middle East Technical University / Türkiye
146.	Recep Şahingöz	Yozgat Bozok University / Türkiye
147.	Recep Zan	Ömer Halisdemir University / Türkiye
148.	Richard J. Cobley	Swansea University / United Kingdom
149.	Robin Jones	University of Bath / United Kingdom
150.	Roland Mainz	Helmholtz Zentrum Berlin, Germany
151.	S. Mansouri	University of Gabès / Tunusia
152.	S. Wageh	Menoufia University / Egypt
153.	Sabit Horoz	Sivas University of Sci. and Technology / Türkiye
154.	Salem El-Faify	Khalid University / Saudi Arabia
155.	Salih Yılmaz	Alparslan Türkeş Sci. and Tech. University/Türkiye
156.	Salim Çerçi	Yıldız Technical University / Türkiye
157.	Sarani Zakaria	Universiti Kebangsaan Malaysia / Malaysia
158.	Savaş Sönmezoğlu	Kahramanoğlu Mehmet Bey University / Türkiye
159.	Seda Beyaz	Balıkesir University / Türkiye
160.	Sedat Şengül	Trakya University / Türkiye
161.	Sefa Ertürk	Niğde Ömer Halisdemir University / Türkiye
162.	Selda Kılıç Çetin	Çukurova University / Türkiye
163.	Sema Yıldırım	Erciyes University / Türkiye
164.	Serap Güneş	Yıldız Technical University / Türkiye
165.	Serap Şentürk Dalgıç	Trakya University / Türkiye
166.	Serdar Aksu	APPLE Inc. / USA
167.	Serdar Sarıçiftçi	Johannes Kepler Linz University / Austria
168.	Sezen Özçelik	Hakkari University / Türkiye
169.	Subhash Chand	National Institute of Technology / India
170.	Şemsettin Altındal	Gazi University / Türkiye
171.	Şükrü Çavdar	Gazi, University / Türkiye
172.	Şükrü Karataş	Kahramanmaraş Sütçü İmam University / Türkiye
173.	T. M. Farag	Al-Azhar University / Egypt
174.	Tamer Abdallah	Ain Shams University / Egypt

175.	Tayyar Güngör	Burdur M. Akif Ersoy University / Türkiye
176.	Thomas Unold	Helmholtz Zentrum Berlin / Germany
177.	Timuçin Emre Tabaru	Sivas University of Sci. and Technology / Türkiye
178.	Tülay Hurma	Eskişehir Technical University / Türkiye
179.	Ursel Bangert	University of Limerick / Ireland
180.	V. Dorozhkin	Kudrinskaja Moscow / Russia
181.	Vasilios Karanikolas	Patras University / Greece
182.	Veysi Güçkan	Çukurova University / Türkiye
183.	Volkan Altunal	Çukurova University / Türkiye
184.	W. Aslam Farooq	King Saud University / Saudi Arabia
185.	Walid Tawfiq Younes	King Saud University / Saudi Arabia
186.	Witold Daniel Dobrowolski	Polish Academy of Sciences / Poland
187.	Wojtek Wlodarski	RMIT University / Australia
188.	Wolfgang Ensınger	Technische Universität Darmstadt / Germany
189.	Y.Azizan – Kalandaragh	Sabalan University of Advanced Tech. / Iranian
190.	Yasemin Çağlar	Eskişehir Technical University / Türkiye
191.	Yasemin Çiftçi Öztekin	Gazi University / Türkiye
192.	Yasemin Şafak Asar	Gazi University / Türkiye
193.	Young Hee	Sungkyunkwan University / South Korea
194.	Z. Lıu	Peking University / China
195.	Zehra Yeğingil	Toros University / Türkiye
196.	Zeki Yarar	Mersin University / Türkiye
197.	Zeyad A. Alahmed	King Saud University / Saudi Arabia

FOREWORD

It is a pleasure for us to offer you Abstracts Book for the 12th international conference on Materials Science and Nanotechnology for Next Generation; MSNG2025. Our goal was to create a scientific platform that introduces the newest results on internationally recognized experts to local students and colleagues and simultaneously displays relevant Turkish achievements to the world. The positive feedback of the community encouraged us to proceed and transform a single event into a conference series. Now, MSNG2025 is honored by the presence of over 150 colleagues from various cities and countries. We stayed true to the original MSNG2025 concept and accepted contributions from all fields of materials science and technology to promote multidisciplinary discussions. The focal points of the conference emerged spontaneously from the submitted abstracts: energy applications, advanced materials, electronic and optoelectronic devices. Further fields of interest include e.g. new advanced and functional materials, advanced-functional composites, biomaterials, smart materials, dielectric materials, optical materials, magnetic materials, organic semiconductors, inorganic semiconductors, electronic materials, graphene, and more.

Our warmest thanks go to all invited speakers, authors, and contributors of MSNG2025 for accepting our invitation, visiting Sivas and using MSNG2025 as a medium for communicating your research results.

We hope that you will enjoy the conference and look forward to meeting you again in one of the forthcoming MSNG2026 event.

Prof. Dr. Ebru Şenadım Tüzemen & Prof. Dr. Fahrettin Yakuphanoğlu

Conference Chairs

FULL TEXT BOOK

Properties of Polypropylene-Based Micro Synthetic Fiber Reinforced Mortars Containing Calcined Marl Blended Cement

Y. Akgün[1]* and C. Özdem Baş[2]

[1] *Department of Construction, Technical Sciences Vocational School, Ordu University, Ordu, Türkiye*

[2] *Institute of Science, Department of Renewable Energy, Ordu University, Ordu, Türkiye*

* ***Corresponding authors:*** ysmakgun@gmail.com

ABSTRACT

Pozzolanic mineral additives, used in appropriate proportions, help to reduce energy consumption and CO2 emissions by reducing the amount of clinker in cement production. Concrete is brittle and has poor ductility under compression. Therefore, concretes exposed to fixed and live loads should be strengthened using fiber. In this work, it was investigated effects on physical and mechanical properties of mortars produced by using both calcined marl blended cement that is an alternative novel pozzolan and polypropylene-based micro synthetic fiber. Calcined marl was replaced with klinker at 0, 10, 20 and 30 wt.% ratios. The polypropylene-based micro synthetic fiber was mixed at different ratios (0.3-0.6 kg/m3) to the mortars. According to results of tests, it was observed that there were positive improvements in the mechanical properties of mortars containing with up 0.6 kg/m3 polypropylene-based micro synthetic fiber and calcined marl blended cement up to 30% replacement ratio. And, the using calcined marl blended cement will contribute to cement production sector in terms of low-emission, energy-saving, low-cost and sustainability.

Keywords: Calcined Marl, Blended Cement, Polypropylene-based Micro Synthetic Fiber, Mortar

1. Introduction

The construction sector is responsible for world energy consumption and greenhouse gas (CO2) emissions. The production processes of cement, which is an essential part of this sector, need new regulations. Cement production is an industrial process that requires intensive use of heat energy. It also accounts for approximately 8-10% of global carbon dioxide emissions and has negative environmental impacts [1]. Replacing a certain portion of cement clinker with mineral additives is the fastest and most effective method and is also economical. Pozzolans are among the most preferred mineral additives because they positively change many properties of concrete, are economical, and could be used in high proportions in concrete composition. Recently, calcined clays and calcined marls have attracted attention. These materials become efficient in the use of additives thanks to their pozzolanic activity after calcination. The mineral content of calcined marls plays an active role in the hydration reactions of cement. With these reactions, calcium silicate hydrate (C-S-H) and calcium aluminate hydrate (C-A-H) components are formed, forming a matrix between the cement grains and enhancing performance in terms of the strength and durability [2]. On the other hand, calcined marls are a suitable alternative mineral additive for sustainable cement production because they are obtained from natural resources and can be processed with low energy [3].

In addition, the tensile strength of concrete also needs to be improved for sustainability. Various types of fiber components are used in the concrete composition to improve the behavioral performance of structural elements under load by improving the weakness of concrete in tensile stresses and controlling the crack mechanism. In this regard, the most commonly used and best-performing are polypropylene fibers.

The aim of this study is to investigate the properties of polypropylene-based micro synthetic fiber reinforced mortars containing calcined marl blended cement.

2. Experimental Details

In this study, CEM I 42.5 R type cement and CEN standard sand were used as fine aggregate. The natural marl used as cement replacement material was supplied from Sinop/Erfelek in the Black Sea Region. In tests conducted to determine the pozzolanic activity of natural marl, according to TS 25 [4], the 7-day average compressive strength of lime-pozzolan mixture samples was 8.10 MPa. The total SiO_2+Al_2O_3+Fe_2O_3 oxides by weight was 76.43%. And, the Blaine value was 4630 cm^2/g [3]. With these values, natural marl meets the pozzolan requirements of TS 25. Polypropylene-based microsynthetic fibers were used in the samples produced in this study. The fibers has a specific gravity of 0.91 g/cm3, a fiber diameter of 0.18 μm, a fiber length of 6 mm, a specific surface area of 250 m2/kg, a tensile strength of 300-400 MPa, and a modulus of elasticity of ~4000 MPa. Fibers were added to the mixtures at amounts of 0.3-0.6 kg/m3. The mixing water was of drinking water quality. In the mortar samples, polycarboxylate ether-type superplasticizer was used at rates of 0.8, 1, 1.1, and 1.2% of the cement weight. Mortar sample labels were determined as PC; Portland Cement, M; Marl, 0, 10, 20 and 30; the first code indicates the calcined marl replacement ratios, 03 and 06; the second code indicates the fiber amounts. Accordingly, in the study; mortar samples containing pozzolanic natural marl mineral additives calcined at optimum temperature and polypropylene-based micro synthetic fiber reinforced mortars and traditional mortars were produced. Flexural and compression test samples were produced with prismatic (40x40x160mm) and cubic (50x50x50mm) molds, respectively. The tests were conducted on the samples to determine mini-slump, density, water absorption, ultrasonic pulse velocity (UPV), flexural strength, and compressive strength. The results from the series of tests were compared within and among themselves. The findings from these comparisons were used to investigate the physical and mechanical performance of mortars produced with calcined marl blended cement and polypropylene-based micro synthetic fiber reinforcement.

3. Results and Discussion:

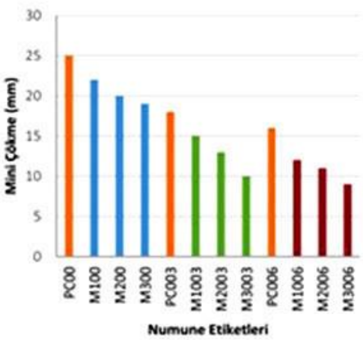

Fig. 1: Mini Slump Values.

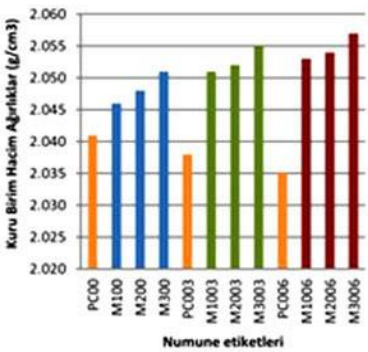

Fig. 2: Dry Density Values.

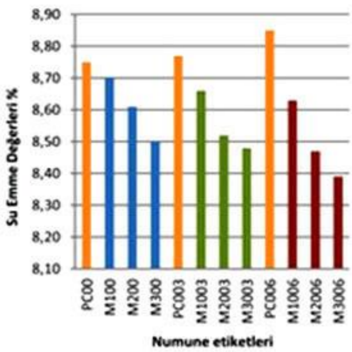

Fig. 3: Water Absorption Values.

The results and discussions of the tests performed on mortar samples are given below. The slump values determined for each mixture in the mini slump tests performed on fresh mortar mixtures are given in Fig. 1. It is observed that as the fiber content of the mortar mixtures increases, the slump values decrease, and with this decrease, workability deteriorates. Although deterioration of workability is considered as an undesirable situation in some cases, it is a desired property in terms of cohesion of plastic mixtures [5]. In the mortar samples containing only calcined marl blended cement and no fibers (PC00, M100, M200, and M300), workability decreased with increasing calcined marl content. However, these decreases were not as severe as those with fiber reinforcement.

Figure 2 shows how the dry densities of 28-days the mortars are affected by the calcined marl blended cement and polypropylene fiber. The densities of mortar samples are affected by properties and densities of mixture components. As the displacement amount of calcined marl added cement increased, the density of the mortars increased due to dense cement paste settling into the voids created by the clumping of the fibers. Polypropylene fibers are not included in mortar mixtures in high quantities and their unit weight is low, so their effect on the increase in mortar density is very small.

The water absorption values for mortar samples are shown in Figure 3. In the tests, water absorption values decreased as the amount of calcined marl increased in the fiber-free series. This decrease is due to the increase in replacement ratio of finer marl content. Additionally, as the calcined marl replacement amount and fiber reinforcement content increased in the fiber and calcined marl series, the water absorption values of the mortar samples decreased. In the fibrous series, it is thought that the voids resulting from the clumping of the fibers is compensated by cement paste with calcined marl blended cement. Polypropylene fibers, which are not water absorbent properties, have a lower effect on water absorption of mortars containing fiber than calcined marl blended cements [6].

The compressive, flexural strength and UPV graphs of mortars are given in Fig. 4, Fig. 5 and Fig. 6. The views of samples used in flexural test are given in Fig. 7. Compressive strength of mortars resulted in an increasing trend depending on the calcined marl and fiber content. However, the compressive strengths of the P003, P006, P02 and P04 series, which do not contain calcined marl, are lower than the compressive strengths of the P00 series due to the absence of calcined marl and the voids created by the fibers [7]. On the other hand, polypropylene fiber reinforcement also improved the flexural strength values of the mortars. These strength results are the results of the 28-day compressive strengths of the mortars, and it is thought that the flexural and compressive strengths of the mortars will increase in later ages thanks to the additional binders developed with the high pozzolanic properties of the calcined marl [8]. The reduction in porosity due to the calcined marl blended cement content of the mortars increases the ultrasonic pulse velocity. The UPV measurement method provides estimated information regarding the porosity and quality of the sample. The variations in UPV values were caused by the calcined marl and polypropylene fibers added to the mixture. The variations in UPVs for all samples showed similar trends to those in compressive strength.

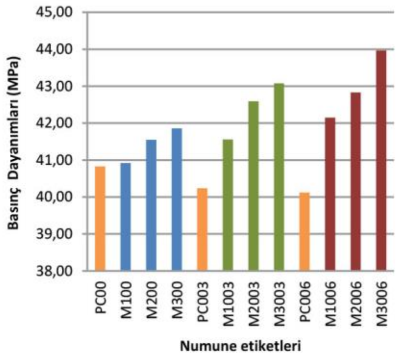

Fig. 4: Compressive Strengths.

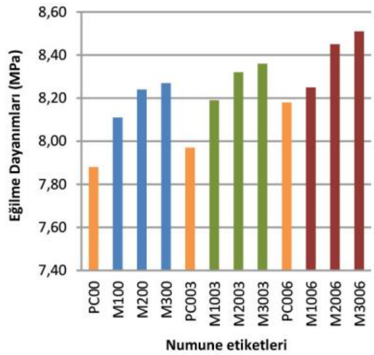

Fig. 5: Flexural Strengths.

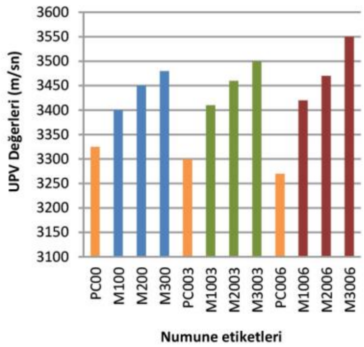

Fig. 6: UPV Variations.

Fig. 7: Appearances of samples after tests.

4. Conclusions

In this study, experimental investigations based on physical and mechanical properties were conducted on mortar samples to improve mortars containing calcined marl blended cement and polypropylene fiber reinforcement. Some of the results obtained from the experimental study are given below.

As in the mortar series containing only polypropylene fibers, in both the calcined marl blended cement and the fiber containing mortar series, the amount of mini-slump decreased due to the changes in fiber and calcined marl.

The densities of the mortar samples in the study decreased only in the fiber containing series. In the series where fiber was used in conjunction with calcined marl, the densities increased due to the filler effect of the calcined marl.

Since the amount of voids in the mortar increases due to the clumping caused by the fibers, water absorption values increase with the increase in the amount of fibers. In series containing cement with fiber and calcined marl blended cement, water absorption values decrease by compensating the voids created by the fibers due to the decrease in cement fineness.

The compressive strengths of the mortar samples showed parallel trends with variations in density. The use of fiber and calcined marl improved the compressive strength of the mortar samples depending on the fiber reinforcement amounts and calcined marl replacement ratios. In the compressive strength findings, the decrease in the strength of the calcined marl blended cement-free series indicates the necessity of using pozzolanic mineral additives to improve the strength of the fiber-containing series. The increase in the strength of mortar samples containing calcined marl blended cement in both non-fibrous and fibrous series is related to the pozzolanic activity developed by the calcination of natural marl, its chemical and mineral content, and its properties such as being ground below the cement fineness [9-11].

In the study, the use of calcined marl blended cement together with polypropylene fiber reinforcements also positively improved the flexural tensile strength of the mortar samples. The results of this experimental study demonstrate that the usable of polypropylene fibers which increase flexural strength due to provide capillary crack control in load-bearing elements.

The variations in UPVs occurred with variations in the amount of calcined marl blended cement and polypropylene fibers in mortar mixtures. The variations of UPVs in all of the mortars showed similar trends to those of strengths.

In summary, according to the results of the experimental study, it was observed that there were positive improvements in physical and mechanical properties of mortars containing up to 0.6 kg/m3 polypropylene fibers and up to 30% calcined marl blended cements.

It has also been determined that the use of mineral additives is inevitable in order to compensate for the voids created by the use of fiber and to improve the performance of the product. Due to the results of this study, the cement industry will be encouraged to use blended cement in terms of low emissions, energy savings, low costs and sustainability.

References

[1] United Nations Environment Programme (UNEP), 2020 Global Status Report For Buildings and Construction: Towards a Zero-Emission, Efficient and Resilient Buildings and Construction Sector, (2020).

[2] Rakhimova, N., Rakhimov, R., Morozov, V., Potapova, L., & Osin, Y. (2021). Marl as a supplementary material to alkali-activated blended cements. European Journal of Environmental and Civil Engineering, 25(13), 2491-2508.

[3] Akgün Y. (2021). Thermal performance of mortars/concretes containing calcined marl as alternative pozzolan. Emerging Materials Research, 10, (3), 246-256.

[4] TSE "TS 25 Natural pozzolan (Trass) for use in cement and concrete-Definitions, requirements and conformity criteria", Turkish Standard Institute, Ankara, Turkey, 2011.

[5] Açıkgenç, M., Arazsu, U., & Alyamaç, K. E. (2012). Farkli karişim oranlarina sahip polipropilen lifli betonlarin dayanim ve durabilite özellikleri. Uluslararası Teknolojik Bilimler Dergisi, 4(3), 41-54.

[6] Ramezanianpour A.A., Esmaeili M., Ghahari S.A. and Najafi M.H. (2013).Laboratory study on the effect of polypropylene fiber on durability, and physical and mechanical characteristic of concrete for application in sleepers, Construction and Building Materials, 44: 411-418.

[7] Song, P. S., Hwang, S., & Sheu, B. C. (2005). Strength properties of nylon-and polypropylene-fiber-reinforced concretes. Cement and concrete research, 35(8), 1546-1550.

[8] Akgün Y. (2020). Behavior of concrete containing alternative pozzolan calcined marl blended cement. Periodica Polytechnica Civil Engineering, 64, (4), 1087-1099.

[9] Danner, T., Norden, G., & Justnes, H. (2018). Characterisation of calcined raw clays suitable as supplementary cementitious materials. Applied Clay Science, 162, 391-402.

[10] Akgün, Y. (2019). Alternatif puzolan kalsine marn içeren sürdürülebilir katkılı çimentolar. Dicle Üniversitesi Mühendislik Fakültesi Mühendislik Dergisi, 10(2), 779-789.

[11] Akgün, Y., & Yazicioglu, Ö. F. (2020). Experimental research on alternative pozzolan analcime to clinoptilolite. Revista Romana de Materiale, 50(4), 502-509.

GaInP/GaAs/Ge Semiconductor Cell Receiver for Fresnel Lens-Based Concentrated Photovoltaic Modules Developments and Performance Analysis

N. Demirtaş Taylan[1], E. Kasapoglu[2], Y. Ozen[3,4], **M.B. Yücel[1*]**

[1] *Department of Physics, Faculty of Science, Akdeniz University, Antalya 07058, Türkiye*

[2] *Department of Physics, Faculty of Science, Sivas Cumhuriyet University, Sivas 58140, Türkiye*

[3] *Department of Physics, Faculty of Science, Gazi University, Ankara 06500, Türkiye*

[4] *Photonics Application & Research Center, Gazi University, Ankara 06500, Türkiye*

[*] ***Corresponding author:***myucel@akdeniz.edu.tr

ABSTRACT

In this study, a Fresnel lens-based concentrated photovoltaic (CPV) module employing GaInP/GaAs/Ge triple-junction semiconductor solar cells was designed and evaluated, with particular emphasis on the development of cell receivers. With the depletion of fossil fuels and the growing impact of environmental challenges, the efficient utilization of solar energy is regarded as a crucial step toward sustainable energy production. Within this context, the development of high-efficiency semiconductor-based solar cells is considered highly significant. Multi-junction III–V cells (GaInP/GaAs/Ge) show higher efficiencies than Si-based cells. A 144-cell CPV panel was fabricated using Fresnel lenses, through which concentrated solar irradiation was directed onto the cells. Aluminum-based receivers were developed, and additional receivers coated with Au, Ag, and Ni were manufactured to assess oxidation under normal atmospheric conditions. Thermal simulations were carried out using SolidWorks, while spectral response and current–voltage measurements were performed experimentally. The triple-junction cells exhibited an open-circuit voltage of 3.1 V, a short-circuit current of 110 mA, and a fill factor exceeding 85%. Long-term outdoor testing indicated that the average panel efficiency remained at ~28%, with oxidation-related efficiency degradation under atmospheric exposure limited to 0.1% over four years. The Fresnel lens structure was found to ensure precise light concentration, while the developed receiver design provided effective passive cooling, preventing thermal losses and structural degradation. In conclusion, the integration of GaInP/GaAs/Ge semiconductor-based triple-junction cells with Fresnel lens concentrators and optimized cell receivers was shown to enable the efficient use of solar energy, while ensuring high efficiency, long-term stability, and cost-effectiveness in next-generation CPV applications.

Keywords: Solar energy, Semiconductor, Triple junction solar cells, Concentrator photovoltaic module, Cell receiver, Fresnel lens, Oxidation

1. Introduction

In multi-junction solar cells, the bandgap E_g sequence is arranged in a decreasing order from the top to the bottom layers. In a triple-junction structure, this sequence follows $E_g(top)>E_g(middle)>E_g(bottom)$. Such an arrangement ensures that high-energy photons are absorbed by the wide-bandgap semiconductor in the top junction, while the remaining photons are subsequently absorbed by lower-bandgap layers beneath, thereby contributing to electricity generation. This stepwise absorption maximizes the utilization of the solar spectrum and enhances overall efficiency. At present, multi-junction technology has advanced up to six junctions, achieving a record conversion efficiency of 47.1% [1,2].

2. Experimental details

The experimental setup consists of 9 Fresnel lenses, each with a lens area of 4X4 cm, and 9 secondary optics aligned along the same optical axis. The spectral responsivity (SR) measurement system, presented in Fig.1, is utilized as one of the experimental characterization methods. This technique serves to determine the regions of the solar spectrum to which the solar cell is sensitive, the specific electromagnetic wavelengths it absorbs, and the efficiency with which it converts the absorbed photons into electrical energy.

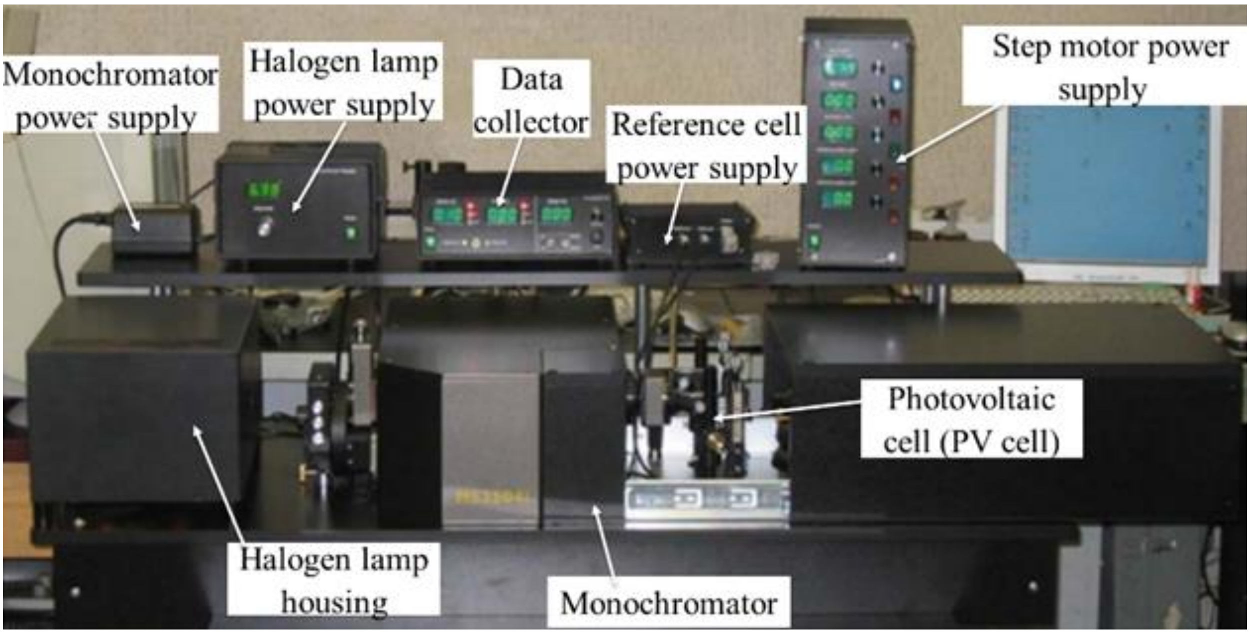

Fig. 1: The general view of the spectral measurement system used in the study is shown. This system consists of a halogen lamp as the light source, a monochromator, a reference cell or detector, and the associated measurement and recording units.

In this study, a concentrator solar panel comprising 144 cells was developed, and TiO_x/AlO_xt hin films were employed as coating materials to minimize surface reflections. The panel incorporates 16 receivers, each containing 9 solar cells. Fig. 2 presents (a) the internal structure and electrical connections of the concentrator solar panel used in the study, and (b) the lens system together with the optical focusing path of the incident rays.

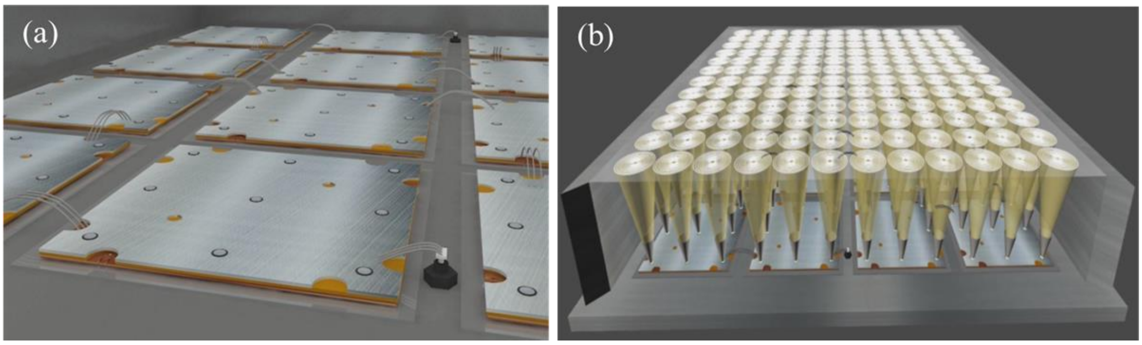

Fig. 2: (a) Internal structure of the concentrator solar panel and the interconnection design between the cells; (b) Optical path of the rays through the lens system of the concentrator solar panel.

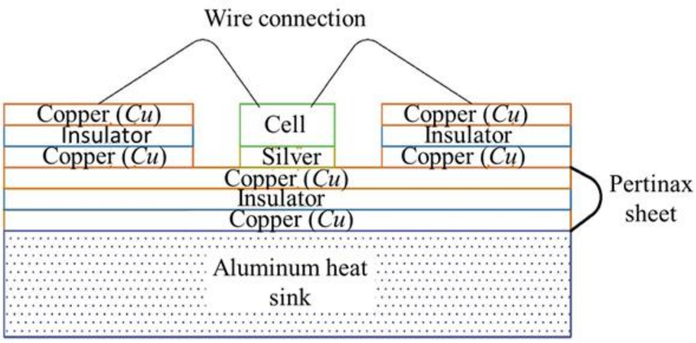

Fig. 3: Schematic of the receiver design.

The receiver system was designed using *Cu* and *Al* plates, with *Au*, *Ag*, and *Ni* coatings applied to mitigate oxidation. A *Cu*–insulator–*Cu* layered Pertinax structure was bonded to an *Al* heat sink using a thermally conductive adhesive to enable passive cooling under high solar concentration. Fig. 3 illustrates the structural integration.

Figures 4(a–c) depict the assembly of the cell receivers into a solar panel. Each receiver contains 9 cells, and their precise alignment is essential in CPV systems to ensure accurate light focusing. Even minor angular misalignments can result in incorrect light concentration.

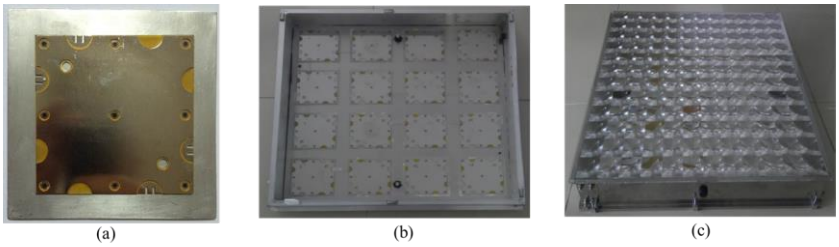

Fig. 4: *(a) The cell receiver mounted onto the Al plate; (b) 16 receivers installed on the Al base; (c) The concentrator photovoltaic panel.*

3. Results and discussion:

As seen in Fig. 5, *GaInP* (blue) operates with ~75% efficiency in the 280–640 nm range, *GaAs* (green) with ~80% in 640–900 nm, and *Ge* (red) with ~70% above 900 nm, together enabling broad-spectrum energy conversion.

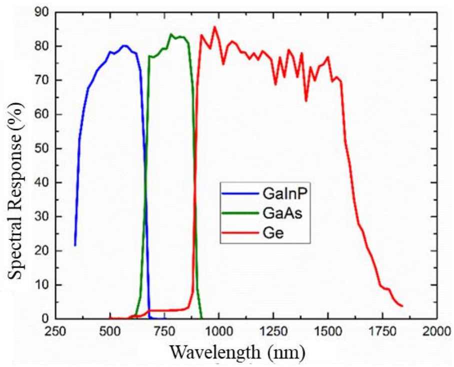

Fig. 5: *Spectral response spectrum of the GaInP/GaAs/Ge triple-junction solar cell.*

The study evaluated the thermal and electrical performance of a CPV panel. Parallel connection of solar cells via conductive plates ensured higher output current, while simulations confirmed that thermal receivers effectively dissipated heat, maintaining cell temperatures around 64 °C (Fig. 6(a)). Temperature distribution analyses showed that insulation between the receivers and the aluminum casing increased cell temperature to 61–62 °C, whereas direct heat flow reduced it to ~59 °C (Fig. 6(b)).

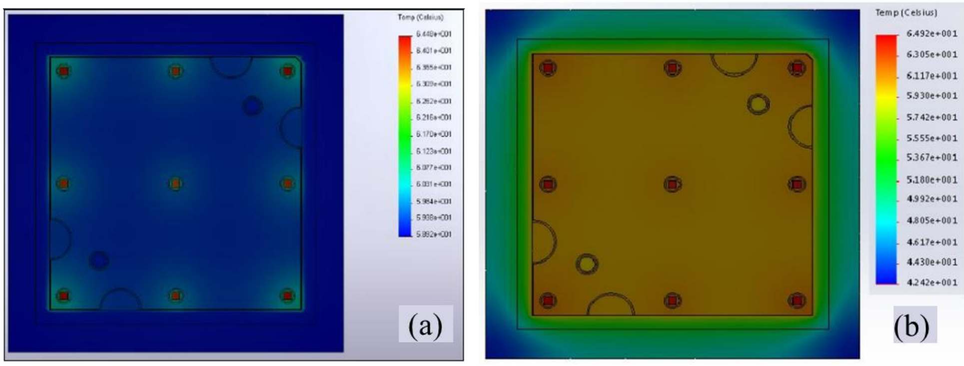

Fig. 6: *Thermal analysis results: (a) Effective absorption of the heat generated by nine solar cells mounted on the receiver; (b) reduced absorption when the receiver is insulated from the outer casing.*

Fig. 7: (a) The cell surface temperature was measured as 84.6 °C without the Al plate;
(b) after placing an Al plate beneath the setup, the cell temperature in the Al-plated receiver system was reduced to 61 °C.

All values measured under 1 Sun using the setup shown in Figure 7(a–b) are presented in Table 1.

Table 1: Temperatures of cells measured under 1 Sun in the environment where the experiment was carried out

System	Temperature (°C)
Room temperature	23,0
Temperature under 1 Sun	38,0
Concentration temperature at the focal length of the Fresnel lens	342,9
Concentration temperature of the secondary optic aligned with the Fresnel lens	250,5
Cell surface temperature without *Al* plate	84,6
Cell surface temperature with *Al* plate	61,0
Temperature on the upper *Cu* surface near the cell (*Al*-plated receiver)	58,3
Temperature at the interface between lower *Cu* surface and *Al* plate	34,2

As shown in Fig. 8, the *GaInP/GaAs/Ge* triple-junction solar cell exhibited an open-circuit voltage of ~3.1 V and a short-circuit current of ~110 mA, consistent with literature [3]. Panel efficiency measurements over four years showed only ~0.1% negligible loss. Outdoor tests under standard conditions revealed that efficiency decreased slightly from 27.9% to 27.6%, while power output varied between 57 W and 37 W.

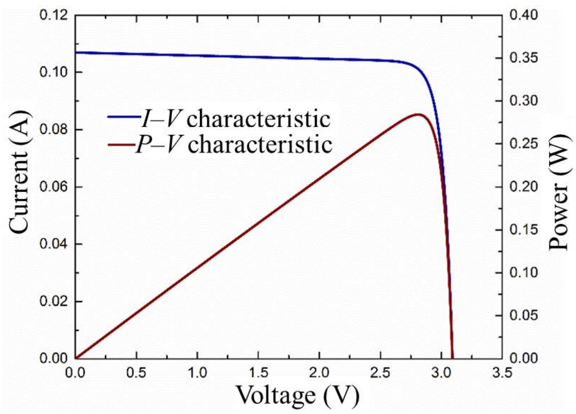

Fig. 8: I–V and P–V characteristics under 1 Sun.

Conclusions

Within the scope of this study, the total output power of the designed and fabricated panel was measured as 60 W. For the concentrator photovoltaic (CPV) panel with a net surface area of 50×50 cm², the power per unit area was calculated to be approximately 240 W/m². Currently, the highest-efficiency silicon-based solar panel used in terrestrial PV applications is the IBC (Interdigitated Back Contact) solar panel, with a power density of around 221 W/m² [4-6]. Considering these values, CPV panel applications represent a promising area for further research and product development. Higher power output can be achieved by designing receiver and lens systems with different geometries and integrating more cells into a given unit area.

Acknowledgement

(i) This work was supported by Presidency of Turkey, Presidency of Strategy and Budget with 2019K12-149045 project number. *(ii)* The authors gratefully acknowledge the financial the support of the Scientific and Technological Research Council of Türkiye (TUBITAK) under the grant no 3130545. *(iii)* Authors gratefully acknowledge the considerable support of CW Enerji Mühendislik Ticaret ve Sanayi A.Ş in Antalya, Türkiye.

References

[1] J.F. Geisz, M.A. Steiner and et al. IEEE J. Photovoltaics, 8 (2018) 626–632.

[2] M.A. Green, E.D. Dunlop and et al. *Prog. Photovoltaics Res. Appl.*, 28(2020) 3–15.

[3] A. Erol and N. Balkan, Yarıiletkenler ve Optoelektronik Uygulamaları, Seçkin Yayıncılık 2015., pp. 347.

[4] A. Baju and M. Yarema, Frontiers in Energy Research, 10 (2022) 971918.

[5] N. Hui, T. Sanyal and R. Das, A Brief Review on Solar Photovoltaic: A Key to Sustainable Development © International Academic Publishing House (IAPH), N.R. Madhu, T. Sanyal et. al. (eds.), A Basic Overview of Environment and Sustainable Development [Volume: 3] (2024) 137-151.

[6] Sunpower 2019. SunPower A-Series 400-425 W Residential Module Datasheet, https://us.sunpower.com/sites/default/files/sp-a450-440-430-com-pv4s-gen42-ds-en-ltr-532726.pdf

Optimization of FDM 3D Printer Parameters: An Experimental and Data-Driven Investigation on Tensile Strength and Surface Roughness with PETG Filament

A. Kaptan[1*]

[1] *Department of Motor Vehicles and Transportation Technologies, Sivas Vocational School of Technical Sciences, Sivas Cumhuriyet University, Sivas 58140, Turkey*

[*] ***Corresponding authors:*** *akaptan@cumhuriyet.edu.tr*

ABSTRACT

This study systematically demonstrates the effects of critical process parameters on mechanical performance (tensile strength, σ) and surface roughness (Ra) during FDM 3D printing using PETG filament. A Taguchi L27 orthogonal array was used for experimental planning, and three levels of layer thickness (0.12–0.28 mm), fill rate (20–80%), printing speed (40–80 mm/s), nozzle temperature (220–250 °C), and scanning angle (0°–90°) were investigated. Samples were produced on a FlashForge Adventurer 5M Pro printer with a 0.4 mm diameter nozzle and subjected to tensile tests according to ASTM D638 Type V. Ra measurements were evaluated using the ISO 4287 (cut-off 0.8 mm) approach. The multi-criteria objective (σ↑, Ra↓) was combined with the desirability approach, and a single optimum setting was reported. OLS-based impact assessment (adj. R^2=0.990, Ra model adj. R^2=0.974) was used for non-categorical parametric analysis, and Random Forest (5-fold cross-validation) was used for estimation (R^2≈0.47 for σ; R^2≈0.32 for Ra). The findings show that the combination of thinner layer, lower speed, nozzle temperature around 250 °C, and 0° scan angle increases σ while decreasing Ra; the fill rate has a positive but limited effect on σ, with a secondary effect on Ra. The recommended optimum parameters are 0.12 mm layer thickness, 80% fill rate, printing speed of 40 mm/s, nozzle temperature of 250 °C, and 0° scan angle.

Keywords: FDM, ANOVA, multi-criteria optimization, surface roughness, tensile strength, machine learning.

1. Introduction

Additive manufacturing (AM) is an innovative manufacturing technology that has found a wide range of industrial applications in recent years, from prototyping to final product production, and stands out with its design freedom, material efficiency, and customization possibilities [1,2]. One of the most widely used methods among these technologies is the Fused Deposition Modeling (FDM) process, which is based on the layer-by-layer deposition of thermoplastic filaments [3]. The low cost of FDM, its easy accessibility at office and laboratory scales, and its compatibility with different engineering polymers are the main factors increasing the prevalence of the method [4]. However, the mechanical performance (e.g., tensile strength, σ) and surface quality (Ra) of parts produced by FDM are often lower than those of parts produced by traditional manufacturing methods [5,6]. This makes the systematic optimization of process parameters critical, especially when it comes to functional prototypes and end-use parts. Studies in the literature reveal that parameters such as layer thickness, infill ratio, printing speed, nozzle temperature, and scan angle directly affect the final part properties [7–9]. However, there are complex interactions between these parameters, and changing a single parameter can lead to opposing effects on different outputs. For example, low layer thickness improves surface quality but prolongs production time; high infill ratio increases tensile strength but increases material consumption and printing time [10]. Among the materials frequently used in the FDM process, Polyethylene Terephthalate Glycol (PETG) stands out with its higher impact strength, lower brittleness, and good chemical resistance properties compared to Acrylonitrile Butadiene Styrene (ABS) and Polylactic Acid (PLA) [11]. Although PETG is increasingly preferred in engineering applications, the majority of studies on parameter optimization have focused on PLA and ABS [12, 13, 14]. In this context, systematic experimental studies using PETG filament have the potential to fill a significant gap in both academic literature and industrial applications.

In this study, the effects of selected critical parameters (layer thickness, infill rate, printing speed, nozzle temperature, and scan angle) on tensile strength (σ) and surface roughness (Ra) in the FDM process using PETG filament were investigated using the Taguchi L27 experimental design. The study was supported by experimental data, multi-criteria optimization (desirability function) and data-driven analysis (OLS regression, random forest model) approaches. Thus, a single optimal parameter set was determined for the use of PETG in FDM, both in terms of mechanical and surface quality, and a more in-depth understanding of the process was developed through parametric and predictive modeling.

2. Material and Method

2.1. Material Used and 3D Printer

In this study, the samples were produced on a FlashForge Adventurer 5M Pro (China, 2023) device (Fig. 1.a), a desktop 3D printer with FDM technology. The printer's technical specifications and basic parameters are summarized in detail in Table 1. Commercially sourced PETG filament (Fig.1.b) was used as the material in the study (diameter: 1.75 mm ±0.05 mm, density: ≈1.27 g/cm³, manufacturer: eSUN, Shenzhen, China). The filaments were dried at 60 °C for 6 hours before printing to prevent the negative effects of humidity during printing.

a b

Fig. 1. FlashForge Adventurer 5M Pro printer and filament.

Table 1. FlashForge Adventurer 5M Pro specifications

Feature	Value
Print Technology	Fused Deposition Modeling (FDM)
Nozzle Diameter	0.4 mm (Adjustable)
Layer Thickness Range	0.08 – 0.40 mm
Print Speed	10 – 300 mm/s (recommended: 40–100 mm/s)
Nozzle Temperature Range	220 – 265 °C
Plate Temperature	110 °C (maks.)
Material Compatibility	PLA, ABS, PETG, ASA, PC vb.
Filament Diameter	1.75 mm

2.2. Experimental Design

To systematically demonstrate the effects of process parameters, the Taguchi L27 orthogonal experimental design was chosen. This method allows five different factors to be evaluated at three levels, reducing experimental overhead and allowing for maximum information to be obtained with a minimum number of experiments. The factors and their corresponding levels are detailed in Table 2. A total of 27 different experimental conditions were applied within the scope of the study and statistical reliability was ensured by performing three repetitions for each condition.

Table 2. Experimental factors and their levels (Taguchi L27 design)

Factor No	Factor	Level 1	Level 2	Level 3
1	Layer thickness (mm)	0.12	0.20	0.28
2	Infill ratio (%)	20	50	80
3	Print speed (mm/s)	40	60	80
4	Nozzle temperature (°C)	220	235	250
5	Scanning angle (°)	0	45	90

2.3. Sample Preparation and Testing Standards

To ensure standardization in mechanical testing, the geometric design and dimensions of the tensile test specimens were based on the ASTM D638 Type V standard, as shown in Fig. 2. Three replicates were produced for each test condition. Tensile tests were performed on a Zwick/Roell Z010 (10 kN capacity) universal testing machine at a test speed of 5 mm/min. The tensile strength (σ, MPa) obtained from the maximum load was recorded. Surface roughness (Ra): Measured using a Mitutoyo Surftest SJ-210 profilometer with a cut-off value of 0.8 mm according to the ISO 4287 standard. Three different points were measured on each specimen, and the average value was calculated.

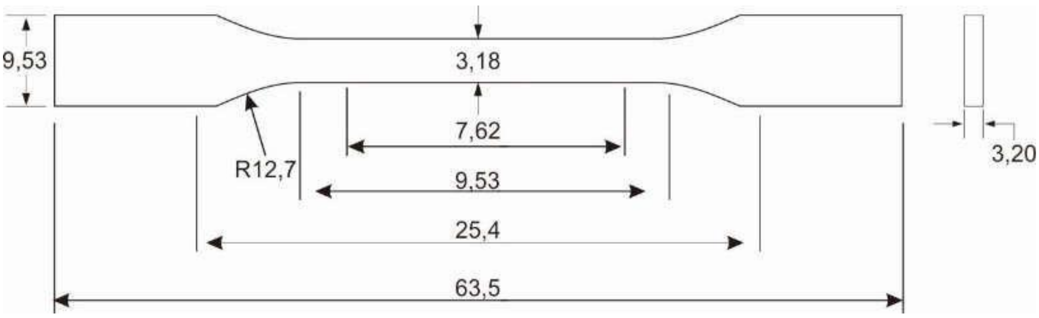

Fig. 2. Test sample geometric design and dimensions (ASTM D638 Type V)

2.4. Statistical Analysis of Experimental Design

Analysis of Variance (ANOVA): Statistical significance of parameters on σ and Ra was evaluated. Regression Analysis (OLS): Parametric relationship modeling was performed. Machine Learning: Random Forest regression model was applied to estimate the parameter-output relationship. The model was tested with 5-fold cross-validation. Multi-Criteria Optimization: Desirability function was applied to maximize tensile strength and minimize surface roughness.

2.5. Experiment Matrix

The experimental design used in this study is based on the L27 orthogonal array, based on the Taguchi approach. The parameter combinations are summarized in detail in Table 3. This table systematically presents the experimental conditions where key process parameters such as layer thickness (LT), infill density (ID), printing speed (PS), nozzle temperature (NT), and scanning angle (SA) are combined at different levels and forms the primary data source for subsequent analyses.

Table 3. Taguchi L27 test matrix

Exp. No	LT (mm)	ID (%)	PS (mm/s)	NT (°C)	SA (°)	Tensile Strength (MPa)	Surface Roughness (μm)
1	0.12	20	40	220	0	44.8	5.5
2	0.12	20	60	235	45	46.2	5.8
3	0.12	20	80	250	90	42.1	6.9
4	0.12	50	40	235	90	48.5	5.2
5	0.12	50	60	250	0	51.0	5.0
6	0.12	50	80	220	45	45.3	6.0
7	0.12	80	40	250	45	52.7	4.8
8	0.12	80	60	220	90	47.2	5.6
9	0.12	80	80	235	0	53.5	4.7
10	0.20	20	40	235	0	42.0	7.5
11	0.20	20	60	250	45	43.7	7.0
12	0.20	20	80	220	90	38.5	8.8
13	0.20	50	40	250	90	45.2	6.9
14	0.20	50	60	220	0	46.8	6.5
15	0.20	50	80	235	45	41.9	7.7
16	0.20	80	40	220	45	48.9	6.3
17	0.20	80	60	235	90	44.6	6.8
18	0.20	80	80	250	0	49.8	6.1
19	0.28	20	40	250	90	37.8	9.5
20	0.28	20	60	220	0	40.5	9.0
21	0.28	20	80	235	45	36.9	10.2
22	0.28	50	40	220	45	42.2	8.4
23	0.28	50	60	235	90	39.1	8.9
24	0.28	50	80	250	0	43.0	8.2
25	0.28	80	40	235	0	46.5	7.9
26	0.28	80	60	250	45	44.0	8.0
27	0.28	80	80	220	90	41.2	8.7

3. Results and Discussion

3.1. Tensile Strength (σ) Results

When general trends are evaluated, decreasing layer thickness (0.12 mm), decreasing printing speed (40 mm/s), and choosing a nozzle temperature of approximately 250 °C stand out as the most critical conditions that significantly increase tensile strength. While the 80% fill rate provided the highest σ value, the effect of this rate was more limited compared to the layer thickness, printing speed, and temperature parameters. At the scanning angle, the 0° orientation strengthened material integrity by creating a fiber-like structure aligned with the load direction and allowed for the highest tensile strength. Fig. 3 shows the average effects of the parameters on tensile strength. Fig. 4 shows a box plot showing the distribution of repeated measurements. Fig. 5 shows the order of parameter significance according to ANOVA statistical analysis. Accordingly, layer thickness has the highest effect, while nozzle temperature has the lowest effect.

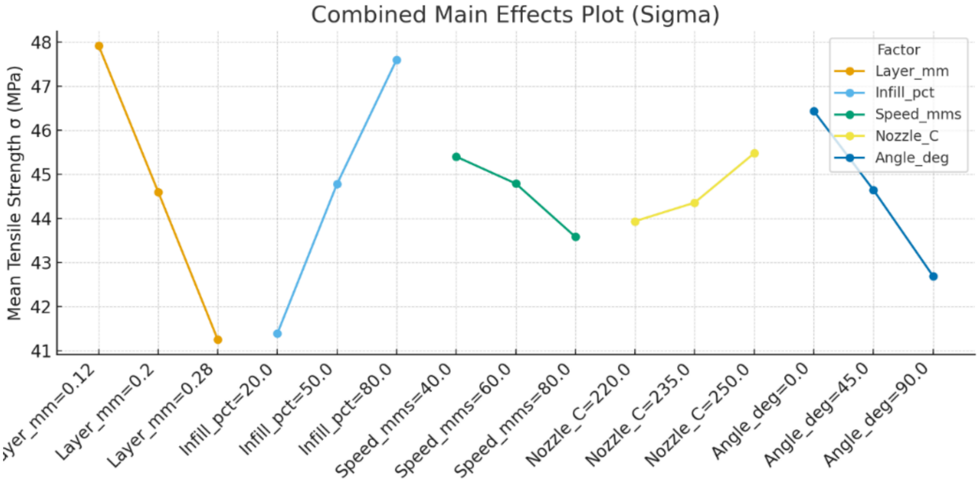

Fig. 3. Main Effects Plot: Average effect of parameters on tensile strength.

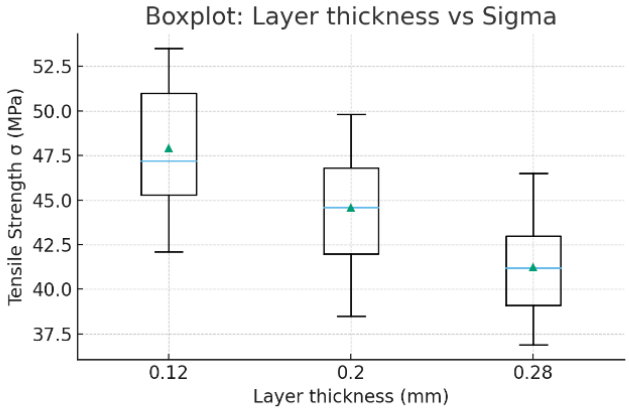

Fig. 4. Boxplots: To show the distribution of repeated measurements.

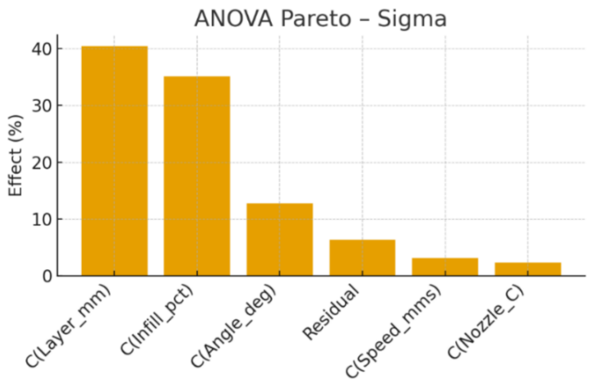

Fig. 5. ANOVA Pareto Chart: To visualize parameter importance order.

3.2. Surface Roughness (Ra) Results

Evaluations of surface roughness (Ra), as seen in Fig. 6, show that layer thickness is the most dominant factor, with the lowest Ra values achieved at a layer thickness of 0.12 mm. Regarding the printing speed parameter, it was determined that lower speeds allow for more controlled material deposition, resulting in a smoother surface. Surface roughness is significantly minimized by achieving optimum melting and flow conditions at a nozzle temperature of around 250°C. While fill rate has a secondary effect on Ra, it is a supporting parameter contributing to print quality. From a scanning angle perspective, better surface continuity is achieved at the 0° orientation, resulting in a reduced number of traces between layer transitions, resulting in higher surface integrity. A box plot showing the distribution of repeated measurements is given in Fig. 7. Fig. 8 shows the order of parameter importance according to ANOVA statistical analysis.

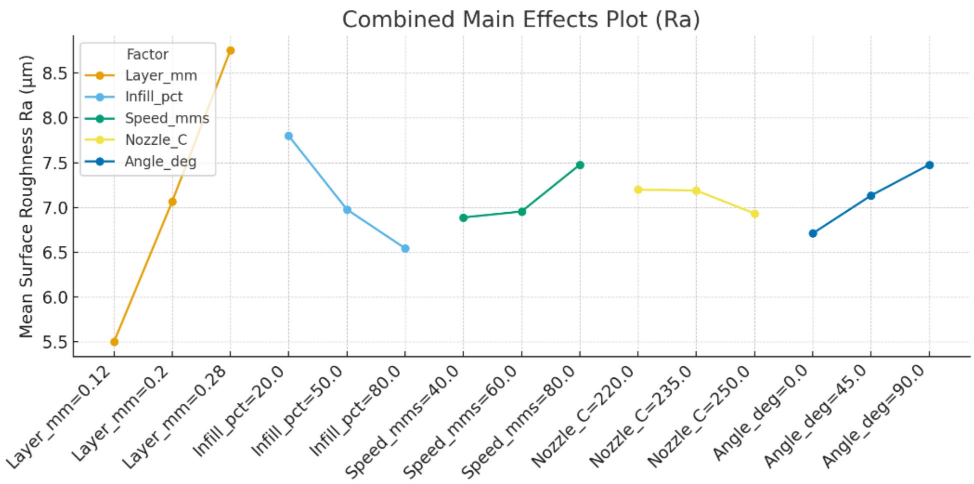

Fig. 6. *Main Effects Plot: Average effect of parameters on Surface roughness (Ra).*

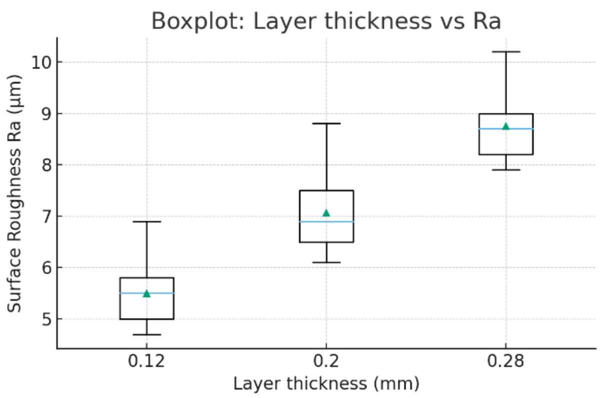

Fig. 7. *Boxplots: To show the distribution of repeated measurements.*

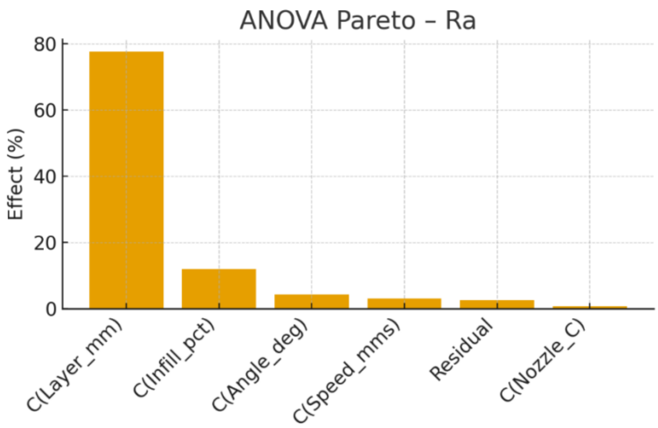

Fig. 8. *ANOVA Pareto Chart: To visualize parameter importance order.*

3.3. ANOVA Results

Table 4 presents the ANOVA analyses performed for tensile strength. The results show a significant distribution of effect sizes among the parameters. Layer thickness had the strongest effect at 40.4%, followed by infill rate, which contributed 35.1%. Scan angle was also found to be statistically significant with a 12.7% effect, demonstrating that it is a significant parameter affecting print quality. In contrast, printing speed showed limited statistical significance at p=0.0408 with an effect size below 3.1%. Nozzle temperature contributed only 2.3% and was not considered statistically significant at p=0.0834, exceeding the significance level of α=0.05. These findings clearly demonstrate that layer thickness and infill rate, in particular, play a decisive role in quality and performance outcomes in the FDM 3D printing process.

Table 4. ANOVA for tensile strength (σ)

Factor	SS	DoF	F-value	p-value	Effect (%)
Layer Thickness	200.67	2	50.98	0.0000	40.4
Infill Rate	174.08	2	44.23	0.0000	35.1
Print Speed	15.48	2	3.93	0.0408	3.1
Nozzle Temperature	11.47	2	2.91	0.0834	2.3
Scan Angle	63.14	2	16.04	0.0002	12.7
Residual Error	31.49	16	–	–	6.3

Table 5 presents the ANOVA analyses performed for surface roughness. Accordingly, layer thickness has the largest effect at 77.6%, while nozzle temperature has the smallest effect at 0.7%.

Table 5. ANOVA for surface roughness (Ra)

Factor	SS	DoF	F-value	p-value	Effect (%)
Layer Thickness	47.72	2	250.16	0.0000	77.6
Infill Rate	7.32	2	38.38	0.0000	11.9
Print Speed	1.87	2	9.81	0.0017	3.0
Nozzle Temperature	0.41	2	2.15	0.1492	0.7
Scan Angle	2.65	2	13.91	0.0003	4.3
Residual Error	1.53	16	–	–	2.5

3.4. Regression and Machine Learning

According to the modeling results obtained, the OLS regression analysis showed an extremely high fit; as seen in Fig. 9 for σ, the value of adj. R^2=0.990 reveals that the parameters explain the tensile strength with almost full accuracy, while as seen in Fig. 10 for Ra, the value of adj. R^2=0.974 indicates that surface roughness can also be predicted quite robustly. In contrast, the machine learning-based Random Forest model exhibited more limited performance; a value of $R^2 \approx 0.47$ for σ partially captured nonlinear effects, and $R^2 \approx 0.32$ for Ra indicated that surface roughness had a more complex and difficult-to-predict character. These results indicate that the classical regression approach is superior in explaining the experimental parameter-output relationship, but that in the presence of nonlinear dynamics, machine learning methods are open to further improvement through different combinations.

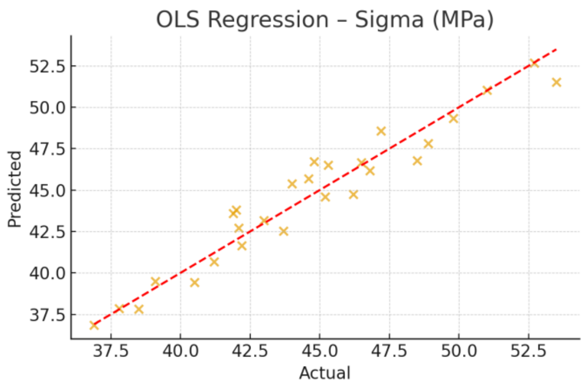

Fig. 9. Estimation of tensile strength (σ) by OLS regression: Comparison of actual and predicted values (R^2_adj ≈ 0.99).

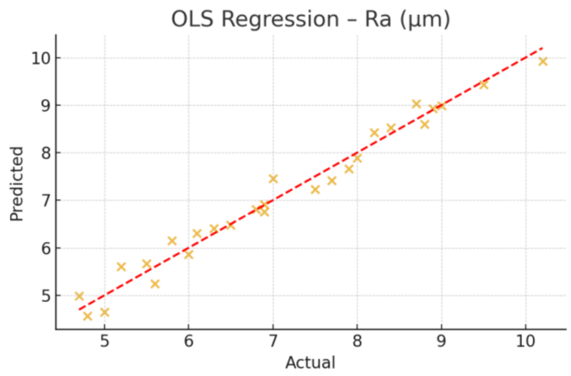

Fig. 10. Surface roughness (Ra) estimation by OLS regression: Comparison of actual and predicted values (R^2_adj ≈ 0.97).

3.5. Multi-Criteria Optimization

In the multi-criteria optimization analysis conducted within the framework of the desirability approach, the primary objective was determined to maximize tensile strength (σ) and minimize surface roughness (Ra). As a result of the evaluations carried out in line with this objective, the optimum parameter combination was clearly demonstrated, as shown in Fig. 11. It was demonstrated that the most ideal results could be achieved by setting the layer thickness to 0.12 mm, the infill rate to 80%, the printing speed to 40 mm/s, the nozzle temperature to 250 °C, the scanning angle to 0°. These optimum conditions stand out as critical settings that enable the simultaneous improvement of mechanical performance and surface quality in the FDM-based 3D printing process.

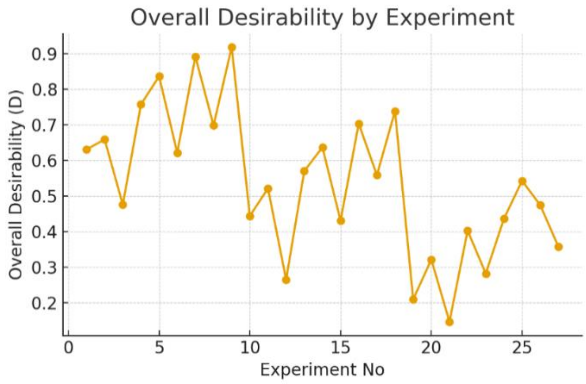

Fig. 11. Desirability chart (multiple objective optimization diagram).

According to the findings presented in Table 6, the optimal parameter combination obtained as a result of multi-criteria optimization within the desirability approach is presented in detail. Accordingly, the optimal printing conditions are defined as selecting a very thin layer thickness of 0.12 mm, maintaining a high infill rate of 80%, adjusting the printing speed 40 mm/s, and setting the nozzle temperature at 250°C. Furthermore, a scanning angle of 0°, maintaining the table temperature at 85°C, and limiting the fan speed to 30% contribute to achieving a balance between performance and quality. When these parameters are evaluated as a whole, the goal is to maximize tensile strength (σ) and minimize surface roughness (Ra). The recommended optimum values are indicative for achieving high quality and reliability in FDM processes.

Table 6. Recommended optimum parameters

Parameter	Optimum value
Layer thickness	0.12 mm
Infill density	%80
Print speed	40 mm/s
Nozzle temperature	250 °C
Scan angle	0°

Conclusions

In this study, the effects of critical process parameters such as layer thickness, infill rate, printing speed, nozzle temperature, and scanning angle on tensile strength (σ) and surface roughness (Ra) were systematically investigated using PETG filament in FDM-based 3D printing technology. A Taguchi L27 orthogonal array was used for experimental planning, and the resulting data were evaluated using both statistical analysis (ANOVA, OLS) and machine learning (Random Forest) approaches.

The main results obtained are:

- Layer thickness was the most critical parameter for both tensile strength and surface roughness.
  - At a layer thickness of 0.12 mm, σ values increased by 15–20%, while Ra values decreased significantly.
- Infill ratio had a positive but limited effect on tensile strength (σ approached maximum at 80% infill). Its effect on Ra was secondary.
- Printing speeds of 40 mm/s yielded optimal results. At higher speeds, σ decreased, while Ra increased.
- Nozzle temperatures of approximately 250°C produced stable results. Interlayer adhesion weakened at lower temperatures, while surface quality deteriorated at higher temperatures.
- The 0° scan angle orientation was determined to provide both the highest σ and the lowest Ra values.
- According to the ANOVA results:
  - The most influential factors for σ were: Layer thickness (40.4%), fill rate (35.1%), and scan angle (12.7%).
  - The most influential factors for Ra were: Layer thickness (77.6%), fill rate (11.9%), and scan angle (4.3%).
- OLS regression had high explanatory power ($R^2\_adj \approx 0.99$ for σ, $R^2\_adj \approx 0.97$ for Ra).
- The Random Forest model performed less well ($R^2 \approx 0.40$–0.50 for σ, $R^2 \approx 0.25$–0.35 for Ra).
- Optimum parameter set obtained through multi-criteria optimization (desirability approach):
  - Layer thickness: 0.12 mm
  - Infill rate: 80%
  - Printing speed: 40 mm/s
  - Nozzle temperature: 250 °C
  - Scanning angle: 0°
- This parameter set provided both high tensile strength and low surface roughness, and was reported as the “single optimum setting” that met the multi-target optimization.

Recommendations and Future Work

- The study is limited to PETG; similar optimization should be conducted on PLA, ABS, and composite-reinforced filaments in future studies.
- Criteria other than tensile strength and surface roughness (e.g., impact resistance, production time, energy consumption) should also be included in multi-criteria evaluations.
- Larger datasets and deep learning methods can be used to improve the performance of machine learning models.
- The obtained optimal parameters should be validated in industrial prototype production and evaluated for sustainability.

References:

[1] Gibson, I., Rosen, D., & Stucker, B. (2021). Additive Manufacturing Technologies: 3D Printing, Rapid Prototyping, and Direct Digital Manufacturing. Springer.

[2] Ngo, T. D., Kashani, A., Imbalzano, G., Nguyen, K. T., & Hui, D. (2018). Additive manufacturing (3D printing): A review of materials, methods, applications and challenges. Composites Part B: Engineering, 143, 172–196.

[3] Turner, B. N., Strong, R., & Gold, S. A. (2014). A review of melt extrusion additive manufacturing processes: II. Materials, dimensional accuracy, and surface roughness. Rapid Prototyping Journal, 20(3), 216–227.

[4] Chacón, J. M., Caminero, M. A., García-Plaza, E., & Núñez, P. J. (2017). Additive manufacturing of PLA structures using fused deposition modelling: Effect of process parameters on mechanical properties and their optimal selection. Materials & Design, 124, 143–157.

[5] Lanzotti, A., Grasso, M., Staiano, G., & Martorelli, M. (2015). The impact of process parameters on mechanical properties of parts fabricated in PLA with an open-source 3-D printer. Rapid Prototyping Journal, 21(5), 604–617.

[6] Mohamed, O. A., Masood, S. H., & Bhowmik, J. L. (2015). Optimization of fused deposition modeling process parameters: A review of current research and future prospects. Advances in Manufacturing, 3, 42–53.

[7] Singh, D., & Sharma, R. (2020). Investigation of effect of process parameters on tensile strength in fused deposition modelling using taguchi method. Materials Today: Proceedings, 21, 1583–1591.

[8] Kalita, K., & Nath, A. (2021). Effect of infill density and infill pattern on mechanical properties of PETG parts fabricated using FDM. Materials Today: Proceedings, 44, 3380–3385.

[9] Carneiro, O. S., Silva, A. F., & Gomes, R. (2015). Fused deposition modeling with polypropylene. Materials & Design, 83, 768–776.

[10] Domingo-Espin, M., et al. (2015). Influence of infill parameters on tensile mechanical behavior in desktop 3D printing. 3D Printing and Additive Manufacturing, 2(4), 183–192.

[11] Vidakis, N., Petousis, M., Velidakis, E., Sagris, D., & Mountakis, N. (2020). A comprehensive investigation of the mechanical behavior and the durability of FDM 3D printed PETG parts. Polymers, 12(5), 1058.

[12] Woehl, T., & Ziegmann, G. (2017). Additive manufacturing with PETG: Influence of process parameters on material properties. Journal of Materials Research, 32(9), 1827–1837.

[13] Ziadia, A., Habibi, M., & Kelouwani, S. (2025). Digital twin-driven real-time optimization of layer-specific surface roughness in FDM 3D printing. Progress in Additive Manufacturing, 1-24.

[14] Aktepe, E., & Ergün, U. (2025). Machine Learning Approaches for FDM-Based 3D Printing: A Literature Review. Applied Sciences, 15(18), 10001.